Micro-liquid enclosure array and its semi-automated assembling system for X-ray free-electron laser diffractive imaging of samples in solution

Takashi Kimura,[1,2,a)] Akihiro Suzuki,[1] Ying Yang,[1] Yoshiya Niida,[1] Akiko Nishioka,[1] Masashi Takei,[1] Jinjian Wei,[3] Hideyuki Mitomo,[1,4] Yasutaka Matsuo,[1] Kenichi Niikura,[1] Kuniharu Ijiro,[1,4] Kensuke Tono,[5] Makina Yabashi,[6] Tetsuya Ishikawa,[6] Tairo Oshima,[7] Yoshitaka Bessho,[6,8] Yasumasa Joti,[5] and Yoshinori Nishino[1,b)]

[1]Research Institute for Electronic Science, Hokkaido University, Kita 21 Nishi 10, Kita-ku, Sapporo 001-0021, Japan.

[2]PRESTO, Japan Science and Technology Agency (JST), 4-1-8 Honcho, Kawaguchi, Saitama 332-0012, Japan

[3]Graduate School of Chemical Sciences and Engineering, Hokkaido University, Kita 13, Nishi 8, Kita-ku, Sapporo 060-8628, Japan

[4]Global Station for Soft Matter, Global Institution for Collaborative Research and Education (GI-CoRE), Hokkaido University, Kita 21 Nishi 10, Kita-ku, Sapporo 001-0021, Japan

[5]Japan Synchrotron Radiation Research Institute/SPring-8, 1-1-1 Kouto, Sayo-cho, Sayo-gun, Hyogo 679-5198, Japan

[6]RIKEN SPring-8 Center, 1-1-1 Kouto, Sayo-cho, Sayo-gun, Hyogo 679-5148, Japan

[7]Institute of Environmental Microbiology, Kyowa-kako Co. Ltd., 2-15-5 Tadao, Machida, Tokyo 194-0035, Japan

[8]Institute of Biological Chemistry, Academia Sinica, 128, Academia Road Sec. 2, Nankang, Taipei 115, Taiwan

a) Current address: Institute for Solid State Physics, The University of Tokyo, 5-1-5 Kashiwanoha, Kashiwa, Chiba 277-8581, Japan

b) Author to whom correspondence should be addressed. Electronic mail: yoshinori.nishino@es.hokudai.ac.jp

We developed micro-liquid enclosure arrays (MLEAs) for holding solution samples in coherent diffractive imaging (CDI) using X-ray free-electron lasers (XFELs). Hundreds of fully isolated micro-liquid enclosures are arranged in a single MLEA chip for efficient measurement, where each enclosure is destroyed after exposure to a single XFEL pulse. A semi-automated MLEA assembling system was also developed to enclose solution samples into MLEAs efficiently at high precision. We performed XFEL-based CDI experiments using MLEAs and imaged in-solution structures of self-assembled gold nanoparticles. The sample hit rate can be optimized by adjusting solution concentration and we achieved a single-particle hit rate of 31%, which is not far from the theoretical upper limit of 37% derived from the Poisson statistics. MELAs allow us to perform CDI measurement under controlled solution conditions and will help reveal the nanostructures and

dynamics of particles in solution.

I. INTRODUCTION

Investigations of nanostructures in solution have importance not only in biology but also in a wide range of scientific and industrial research. The observation should be ideally performed under controlled solution conditions without any fixation, staining, or slicing of the sample. X-rays have a unique advantage that measurement can be done under various environmental conditions due to their high penetrating power and are also effective in imaging nanostructures in solution. Here, liquid cells have key importance in controlling solution conditions in wet X-ray imaging.[1] Liquid cells have been used to image hydrated biological specimens with X-rays in the water window spectral region using Fresnel zone plate objective lenses, and silicon nitride (SiN) membranes have been commonly employed as window materials of liquid cells.[2,3] More recently, liquid cells with SiN windows have been utilized in various kinds of lensless coherent X-ray imaging in the hard X-ray region as well.[4–6] There also exist sophisticated liquid cells that are capable of culturing biological cells internally prior to X-ray measurement by the combined use of SiN windows and a UV-curable adhesive as a moldable material.[7] Moreover, liquid cells have been applied in a wide range of electron microscopy studies.[8] In both X-ray and electron microscopy, radiation damage is a major concern in wet imaging.

Femtosecond-pulsed X-ray free-electron lasers (XFELs) allow us to overcome the radiation damage problem and to take snapshots of intact structures of samples by outrunning major radiation damage processes.[9,10] Coherent diffractive imaging (CDI)[11–13] is a commonly used technique in XFEL nanoimaging of non-crystalline particles, where the sample particles are often delivered using various kinds of injectors.[14–18] Fixed target approaches are also adopted in CDI using XFELs, but those developed by other groups are for either dried[19,20] or frozen-hydrated samples.[21] Though various sample delivery techniques have been developed similarly for serial femtosecond crystallography using XFELs,[22] much lower background scattering is required for CDI because of extremely low X-ray scattering signals from non-crystalline nanoparticles. The introduction of liquid cells makes XFEL based radiation-damage-free CDI also applicable to in-solution nanostructure under controlled solution conditions. Above all, it allows us nanoimaging of biological samples near-physiological conditions at ambient temperature. The solution concentration can be easily controlled in liquid cells to optimize the sample hit rate, which is especially beneficial in using a highly focused XFEL beam and in measuring samples with high scarcity value.

In this paper, we present the design and evaluation of micro-liquid enclosure arrays (MLEAs) for holding solution samples under controlled environmental conditions in CDI using XFELs. Exposure to a single XFEL pulse destroys the solution enclosure of the MLEA. Therefore, to observe multiple intact samples successively, hundreds of fully isolated micro-liquid enclosures are integrated onto a single MLEA chip in contrast to conventional liquid cells with a single enclosure that have been used

in X-ray imaging studies. Each enclosure is separated from its neighbors by a grid partition so that the damage to one enclosure does not affect the others. We performed pulsed coherent X-ray solution scattering (PCXSS) measurement using MLEAs at SPring-8 Angstrom Compact Free Electron Laser (SACLA)[23] to image self-assembled gold nanoparticles (GNPs) in solution. PCXSS is XFEL-based CDI for solution samples.[24,25] The sample solution was enclosed in MLEAs under an ultraclean environment using a semi-automated MLEA assembling system. Each enclosure of MLEAs was exposed to a single XFEL pulse and the coherent X-ray diffraction (CXD) patterns were recorded. The measurement was performed in a vacuum to avoid air scattering noise.[18] The image of a self-assembled GNPs in solution was reconstructed by the combined use of noise-suppression algorithms[26] for CXD data and phase retrieval algorithms.[12]

II. DESIGN OF MLEAs

We developed MLEAs to hold solution samples in PCXSS measurement. The MLEA chip encloses a solution sample in between two thin membranes separating solution sample from the vacuum environment. The membranes act as windows to illuminate the solution sample with an incident XFEL pulse and to pass through the diffracted X-rays. The membrane windows of each micro-liquid enclosure are destroyed with a single shot exposure of a highly intense XFEL pulse. Therefore, a single MLEA chip is desired to have as many micro-liquid enclosures as possible for efficient measurement. The MLEA consists of two substrates stuck together tightly, where each substrate has an array of thin freestanding membrane windows. One of the two substrates has a grid partition to guarantee the independence of each enclosure. The grid partition has a key role in preventing the inner sample solution from evaporation even when an XFEL pulse breaks a neighboring enclosure. The thickness of the partition determines the solution layer thickness and can be determined by considering, *e.g.*, the sample size.

A schematic of an XFEL experiment using an MLEA is shown in Fig. 1(a). Figs. 1(b) and 1(c) show a photograph and a cross-sectional image of an MLEA chip, respectively. The MLEA chip shown in Fig. 1(b) is 14 mm × 14 mm in size and contains 576 enclosures in a 24×24 array. The membrane windows are made of 200-nm-thick SiN and are supported by a 150-μm-thick silicon substrate. The use of thinner silicon substrates can increase the degree of integration of enclosures in a single MLEA, as explained later. However, if silicon substrates are too thin, the risk of breaking them in handling increases. We chose 150 μm as the approximate minimum thickness of silicon substrates with a substantially low risk of breakage in handling.

Homogeneous thin SiN membranes are X-ray transmissive and their flat structure helps diminish the generation of parasitic elastic scattering. Therefore, they are widely utilized as windows in X-ray measurement, including XFEL applications.[1–7,19–22] For 4.0 keV X-rays, the transmittance of two 200-nm-thick SiN membranes is about 0.96, and X-ray absorption is thus negligible. Moreover, in considering an elastic mean free path of 4 keV X-rays of 14 mm for water,[27]

multiple elastic scattering can be neglected (the first-order Born approximation). In this approximation, elastic X-ray scattering occurs at most once, either by sample or solution.

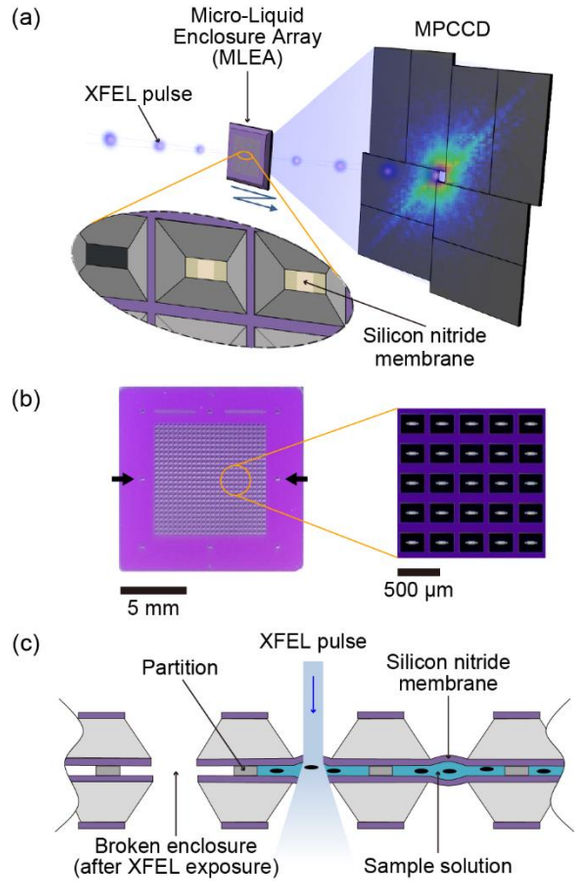

Figure 1: MLEAs for PCXSS measurement. (a) Schematic of PCXSS experiment using MLEAs. A focused XFEL beam illuminates the sample solution in an MLEA and CXD patterns are recorded. (b) Photograph of an MLEA. The 14 mm × 14 mm MLEA has 576 enclosures in a 24×24 array. The arrows indicate alignment marks. (c) Cross-sectional image of MLEA. Micro-liquid enclosures in an MLEA are separated from each other by a grid partition.

Each membrane window of the substrate has a rectangular shape, and we set the size to 80 μm × 20 μm for MLEA shown in Fig. 1(b). The two substrates are to be assembled with a relative in-plane rotation angle of 90° so that their membrane windows cross perpendicularly and form square apertures, each 20 μm × 20 μm in size, when assembled. The crossed arrangement of the two rectangular membrane windows helps gain a greater tolerance for the misalignment of the two substrates.

The size and the thickness of each SiN membrane window were designed also by considering the deflection of the membranes. The pressure exerted by the enclosed sample solution in the vacuum environment makes the thin SiN membranes deflect outward. It is important to minimize the deflection to precisely control the solution layer thickness. The deflection w_{def} of a rectangular

membrane can be estimated by

$$w_{\mathrm{def}} = k\frac{pa^4}{Eh^3}, \tag{1}$$

which is derived from Kirchhoff-Love's theory.[28] Here, p is the pressure applied to the SiN membrane, E is Young's modulus of elasticity of the SiN membrane. a and h are the narrower side width and the thickness of the rectangular SiN membrane, respectively. k is a parameter determined by the aspect ratio of the rectangular membrane and the boundary condition at the membrane edges. When the aspect ratio of the rectangular membrane is larger than 4, k takes a value of about 0.03 under the fixed-end boundary condition.[28] The value of Young's modulus for SiN is 300 GPa.[29] To make the deflection of the 80 μm × 20 μm SiN membrane smaller than 200 nm, the SiN membrane should be thicker than 200 nm.

In the MLEA chip shown in Fig. 1(b), the interval of the two-dimensionally arrayed enclosures is 350 μm in both directions, which is restricted by the anisotropic etching of silicon to be described in detail later. Considering an anisotropic etching angle of 54.7° for the (100) plane of silicon and a rectangular freestanding membrane size of 80 μm × 20 μm to be fabricated, the rectangular pattern on the backside of the 150-μm-thick silicon should have a size of about 230 μm × 290 μm. Considering some gaps between rectangular patterns, we set the interval between enclosures to 350 μm.

III. FABRICATION OF MLEAs

We fabricated the substrates of MLEAs by conventional photolithography. Fig. 2(a) shows the fabrication process of the substrates. 200-nm-thick SiN films were first coated on both surfaces of a 150-μm-thick Si (100) wafer by low-pressure chemical vapor deposition. On one side of the Si wafer, a thin layer of positive photoresist (MicroChem OFPR-2000) was deposited and a two-dimensional array of rectangles was patterned by a mask aligner system (MIKASA MA-20). After a development process, the unmasked regions of the SiN membrane were removed by reactive ion etching (SAMCO RIE-10NRV). Finally, the Si wafer was anisotropically etched with KOH aq. at 80°C. SiN membrane surfaces were then cleaned with wet and dry processes. In the wet-cleaning process, the substrates oscillated up and down in Semicoclean 23 (Furuuchi Chemical) solution, acetone, ethanol, and ultrapure water in sequence. In the dry-cleaning process, O_2 plasma was applied to both sides of the substrates. Here, O_2 plasma can also etch the SiN membranes. Since the increase in the surface roughness of SiN membranes can enhance X-ray scattering from the membrane, which becomes noise in PCXSS measurement, we measured the roughness of the SiN membrane after cleaning. The arithmetic mean roughness R_a of the SiN membrane surface was measured to be below 0.1 nm, which is equivalent to that of Si wafer, indicating that the dry-cleaning process did not enhance the surface roughness of the SiN membrane.

In the lower substrate of the MLEA, we lithographed a grid partition made of thin epoxy-based photoresist (MicroChem SU-8) to separates enclosures from each other. The thickness of the grid

partition was verified to be controlled from 500 nm to a few tens of micrometers by adequately choosing the viscosity of the photoresist and the rotation speed of the spin coater.

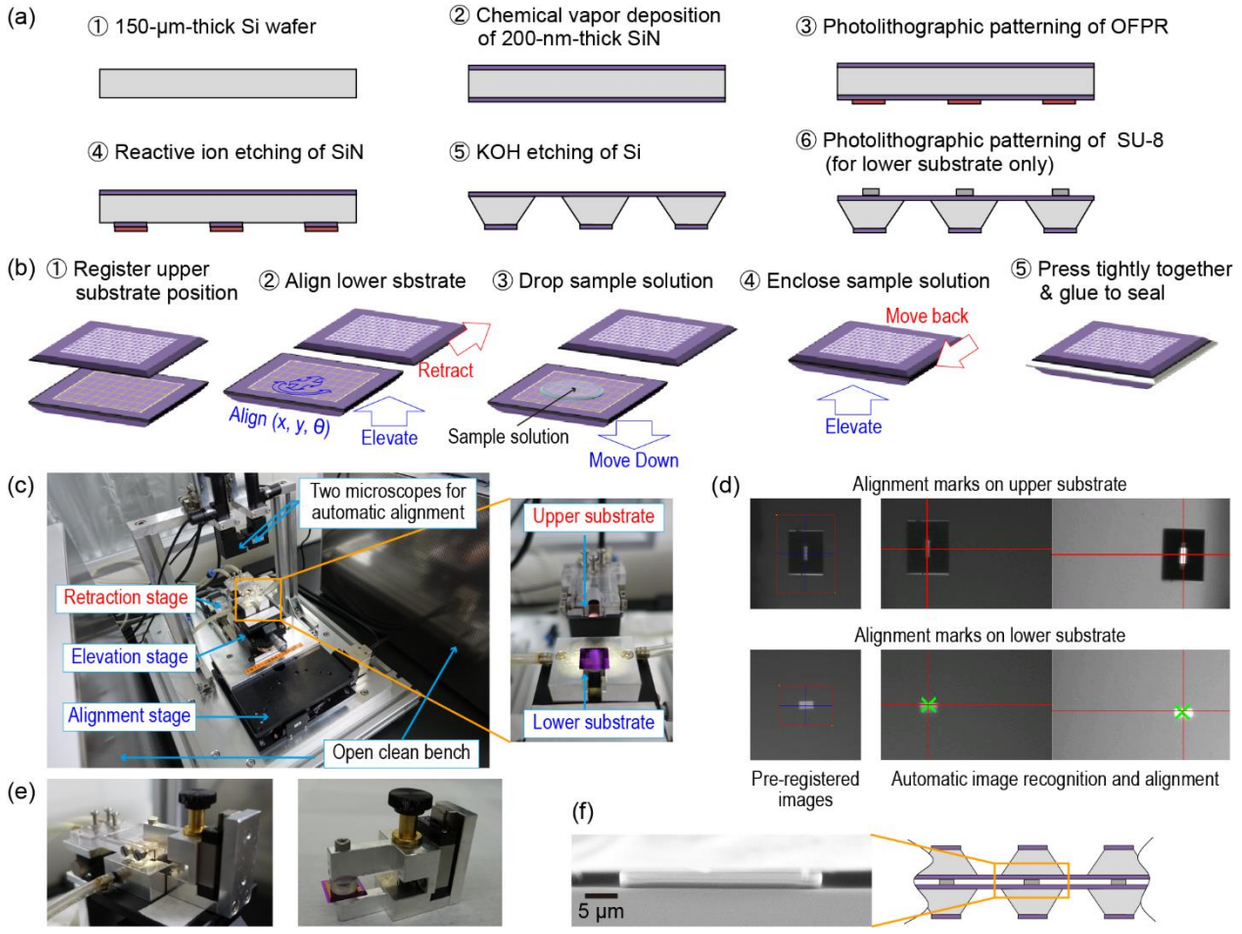

Figure 2: Fabrication and assembly processes of MLEAs. (a) Fabrication process of MLEA substrates. (b) Five main steps to assemble MLEAs. (c) Semi-automated MLEA assembling system. (d) Pre-registered images of the alignment marks on MLEA and the results of automatic image recognition and alignment for (top) the upper and (bottom) lower substrates. (e) Jig to tightly press the upper and lower substrates of MLEAs. (f) Cross-sectional SEM image of the grid partition of MLEA. The MLEA was manually sectioned with a diamond cutter. A 2-μm-thick rectangular-shaped grid partition is visible in between the upper and lower substrates. The scale bar is 5 μm.

IV. ENCLOSING SAMPLE SOLUTION INTO MLEAs

We enclosed the sample solution into MLEA chips at SACLA just before PCXSS measurement. In our early experiments,[24] MLEAs were assembled manually by observing windows through an optical microscope with eyes and aligning two chips with manual stages. We have been gradually developed a semi-automated MLEA assembling system afterward, which made our sample preparation much efficient. Efficiency in sample preparation will become crucially important when performing, *e.g.*, 3D

imaging.

Figs. 2(b) and 2(c) show five steps to assemble MLEAs and pictures of the semi-automated MLEA assembling system, respectively. Open clean benches (KOKEN KOACH T500-F) were used to keep the enclosing work environment clean at class 1 to prevent contamination. For hydrophilic solution samples, the substrates were hydrophilized before the MLEA assembling process.

First, the upper and lower substrates of the MLEA were placed and fixed to vacuum chucks of the semi-automated MLEA assembling system with a relative in-plane rotation angle of 90° as mentioned above. Here, the substrates were fixed with their etched surface facing toward the vacuum chucks, and the vacuum chucks were applied only on the silicon frame, where there were no SiN membrane windows. The precise initial position of the upper substrate was determined by monitoring the two alignment marks (Fig. 1(b)) on the upper substrate with two optical microscopes and by using an image recognition system (FAST Corp. FV-aligner). Fig. 2(d) top shows the pre-registered image of the alignment mark on the upper substrate and the result of automatic image recognition. The upper substrate was then retracted, and the lower substrate was elevated to the in-focus position of the two microscopes. The precise position of the lower substrate was determined by the two microscopes and the image recognition system by monitoring the two alignment marks (Fig. 1(b)) on the lower substrate. The precise amount of misalignment of the two substrates was then immediately calculated, and the XYθ-stages (Hephaist Seiko NAF3C-16K) for the lower substrate automatically corrected the misalignment. Fig. 2(d) bottom shows the pre-registered image of the alignment mark on the lower substrate and the result of automatic image recognition and alignment.

After the alignment of the two substrates, a few microliters of the sample solution was dropped on the lower substrate. The sample solution was then quickly enclosed by the two substrates by moving back the upper substrate to the initial position and elevating the lower substrate until the two substrates were in contact. The enclosing process took less than 10 seconds after dropping the sample solution, which helps avoid the evaporation of a small amount of the dropped sample solution. The jig shown in Fig. 2(e) was then used to hold the aligned two substrates and was detached from the MLEA assembling system after releasing the vacuum of the vacuum chucks. After detaching the jig holding the aligned two substrates, we retighten the screw of the jig by fingers to press the two substrates tightly. For 150-μm-thick silicon substrates, the tightening process is reliable without the worry of breaking them. Finally, the pressed substrates were sealed with a biologically compatible adhesive material. The absence of bubbles in enclosures can be confirmed by observing MLEAs with a digital microscope. Fig. 2(f) shows a cross-sectional image of the assembled MLEA observed with a scanning electron microscope (SEM) (JEOL JSM-6700FT). From the SEM image, we confirmed that the gap between the two substrates was equivalent to the thickness of the partition.

V. EVALUATION OF MLEAs

We evaluated the deflection and the endurance of SiN membranes of MLEAs by applying

atmospheric pressure using the equipment shown in Fig. 3(a). We measured the surface deflection profile of the SiN membrane with a Mirau interferometer (Zygo Corporation, New View 7300) with keeping one side of the SiN membrane under vacuum. The measured profile of the surface deflection for a 20 μm × 80 μm × 200 nm SiN membrane is shown in Fig. 3(b). The maximum deflection was about 200 nm, which agrees well with the theoretical calculation using Eq. (1). The SiN membrane did not break, and the deflection was not changed during the experiment for more than one hour.

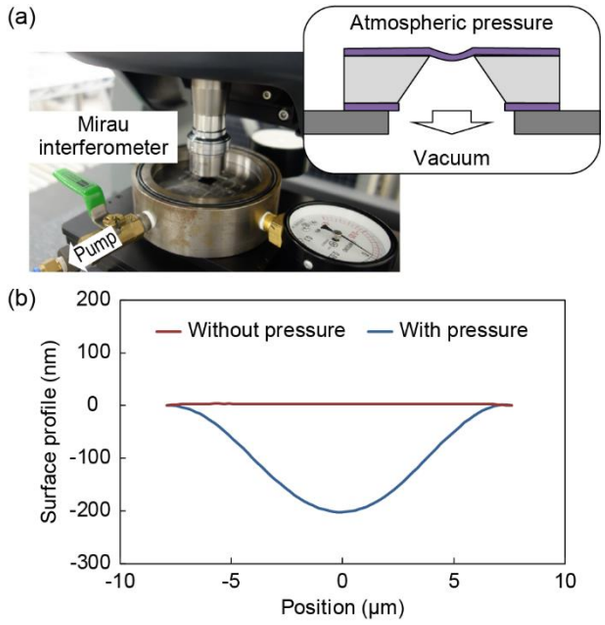

Figure 3: Deflection and endurance tests of MLEAs. (a) Setup of the test measurement (b) Deflection profile of the SiN membrane.

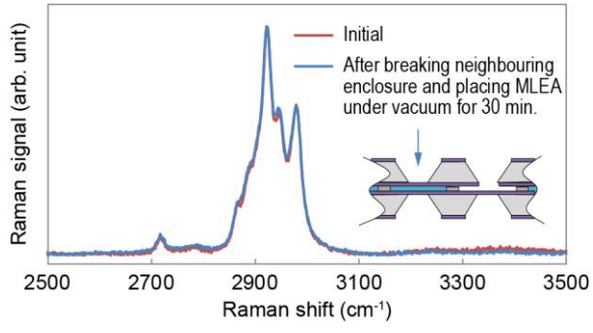

Figure 4: Butanol solution sealing test using a Raman microscope. The Raman spectra of an enclosure of an MLEA in the initial intact condition and the same enclosure after manually breaking a neighboring enclosure and placing the MLEA under a vacuum for 30 minutes. The butanol peaks observed in both spectra overlap almost perfectly, which justifies the independence of each enclosure of MLEAs.

We verified the presence of the sample solution in MLEA under vacuum by measuring the

spectrum of the enclosed butanol solution with a Raman microscope (Renishaw inVia Reflex). We utilized butanol because the Raman spectrum of C–H bonds can be easily detected with Raman spectroscopy. First, we measured a Raman spectrum of an intact enclosure of an MLEA. We then manually broke the SiN membrane of a neighboring enclosure by a sharp pin and placed the MLEA under a vacuum for 30 minutes to simulate damage by XFEL exposure. Thereafter, Raman microscope measurement was performed again to the same enclosure that was initially measured. Fig. 4 shows the Raman spectra of the enclosure before and after breaking a neighboring enclosure and placing the MLEA under a vacuum. Both spectra overlap almost perfectly and show strong Raman peaks from the C-H bond around 2950 cm^{-1}. This result proves that sample solution can be preserved in MLEA chips without evaporation even when a neighboring enclosure is destroyed.

VI. PCXSS EXPERIMENT

We performed a PCXSS experiment using MLEA at the beamline 3 of SACLA. The XFEL pulses from SACLA, with a photon energy of 4.0 keV and a pulse duration of shorter than 10 fs, were coherently focused to a spot size of 1.5 μm × 1.6 μm.[30] MLEA chips were mounted at the focus in the Multiple Application X-ray Imaging Chamber (MAXIC).[31] Accurate positioning of MLEA is required because each aperture of MLEAs is as small as 20 μm × 20 μm. We aligned MLEA chips to the focused XFEL beam by using a retractable on-axis zoom lens camera. In the alignment process, we first exposed the silicon frame of the MLEA to a single XFEL pulse and marked the damaged spot position on the monitor screen of the zoom lens camera. By using the mark on the monitor screen, we determined the coordinates of the enclosures at the four corners. These coordinates were used to determine the coordinates of all other enclosures by interpolation. In synchronization with the movement of the stepping motor stages to each enclosure position, an XFEL pulse selector was opened to allow the exposure of each enclosure to a single XFEL pulse. Single-shot CXD patterns were recorded with a multi-port charge-coupled device (MPCCD) detector[32] located 1.52 m downstream of the sample. MPCCD has 2048 × 2048 pixels, each of which has a size of 50 μm × 50 μm. The measured CXD patterns were visualized online by the prompt data analysis system at SACLA.[33]

We measured self-assembled vesicles of GNPs in dioxane containing 4% water.[34] The sample has been developed aiming to utilize as a stimuli-responsive drug delivery carrier or an enhancer in surface-enhanced Raman scattering and was prepared via self-assembly of 30 nm-diameter GNPs with carboxylic acid-terminated fluorinated oligo(ethylene glycol) ligands.[34,35] Fig. 5(f) shows a scanning transmission electron microscope (STEM) image (Hitachi HD-2000) of dried self-assemblies composed of 30 nm particles measured in the transmission electron (TE) mode. Though electron microscopy usually provides dried structures only, the in-solution structure is critical in optimizing the material design.

With MLEAs, one can easily adjust the solution concentration to optimize the hit rate without

worrying about clogging. In the measurement, a single-particle hit rate of 31% and a multiple-particle hit rate of 6% were achieved. The result was obtained by shooting 23×23=529 enclosures out of a total of 24×24=576 enclosures of an MLEA with XFEL pulses, which gave 165 single-particle hits and 33 multiple-particle hits. Here, one row and one line were not shot with XFEL pulses intentionally in case we need to check unshot enclosures afterward. The hit rate is expected to obey Poisson's statistics, and our result corresponds to a mean particle number of about 0.53 intercepted by single XFEL pulses. The theoretical upper limit of the single-particle hit rate is 37%, where the mean number of particles intercepted by single XFEL pulses is 1: For the Poisson distribution for the number of events m with mean x, $P_x(m) = x^m e^{-x}/m!$, the probability to get $m = 1$ has the maximum value of $1/e \approx 0.37$ at $x = 1$. Our result is not far from the theoretical upper limit.

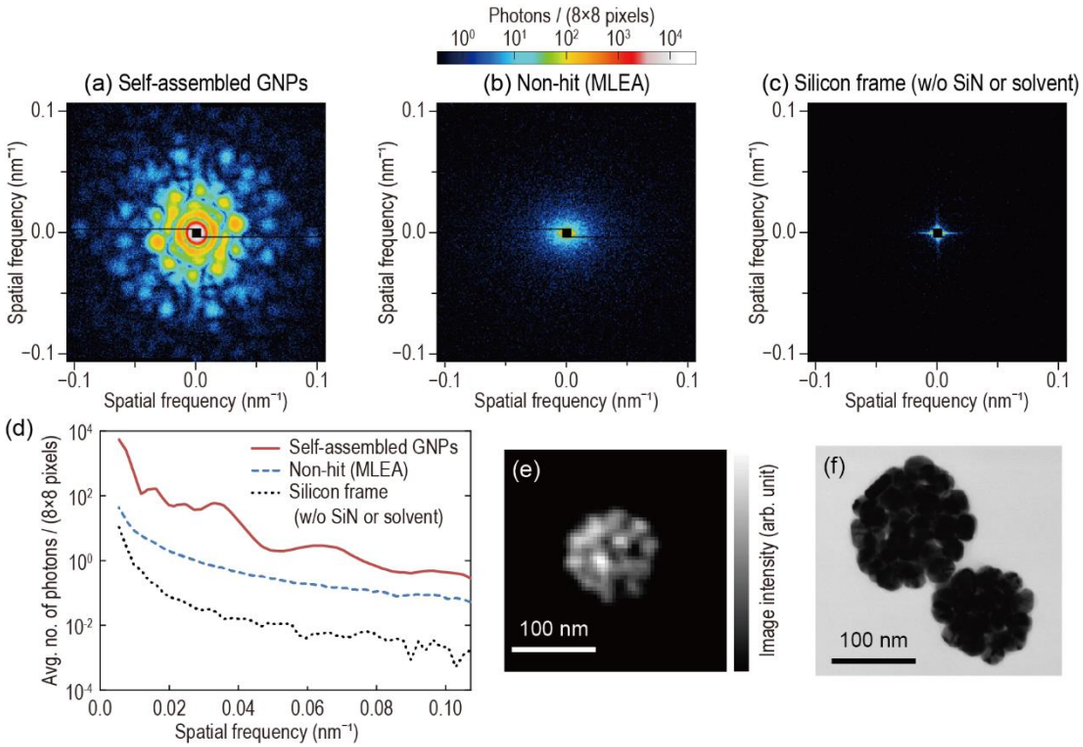

Figure 5: PCXSS imaging result for self-assembled GNPs. The self-assembly consists of 30-nm-diameter GNPs coated with carboxylic acid-terminated fluorinated oligo(ethylene glycol) ligands. (a) CXD pattern from self-assembled GNPs. (b) Non-hit scattering pattern originating from an MLEA with the enclosed solvent (c) Scattering pattern from an MLEA without SiN membrane windows (silicon open aperture). (d) Circular averages of (a)–(c). (e) In-solution image of self-assembled GNPs reconstructed from the CXD pattern in (a). (f) STEM image (TE mode) of dried self-assemblies of the same kind.

In CDI, faithful image reconstruction requires CXD data with low noise. The noise level of the MPCCD is lower than the single-photon counts of 4 keV X-rays, thus the MPCCD signal can be

digitized into the photon counts to suppress the noise. In the present measurement, the centrosymmetric nature of the CXD patterns can also be utilized in considering negligible X-ray absorption and negligible curvature of the Ewald sphere. Fig. 5(a) shows a single-shot CXD pattern of a self-assembled GNPs after digitization, centrosymmetrization, and 8×8 binning. A non-hit scattering pattern originating from an MLEA with the enclosed solvent is also presented in Fig. 5(b). Furthermore, in Fig. 5(c) we display a scattering pattern from an MLEA without the SiN membrane windows, *i.e.* a silicon open aperture, placed at the XFEL beam focus. Figs. 5(a) and 5(b) show no effect of breakage of the enclosure and demonstrate that the single femtosecond XFEL pulses can capture snapshots of intact structures, supporting previous XFEL experiments.[10] Although the SiN membranes and solvent produced some scattering noise as the circular averages of Figs. 5(a)–(c) are shown in Fig. 5(d), the scattering noise was smaller than the signal from the self-assembled GNPs even at the highest scattering angle. Further reduction of scattering noise from the membrane windows is required when measuring weaker X-ray scatterers.

The image reconstruction was carried out for the CXD pattern in Fig. 5(a) for demonstration. The reconstruction algorithm consists of two steps as reported previously.[24] In the first step, we used the relaxed averaged alternating reflections algorithm[36] with shrink-wrap support[37] to determine the support to be used in the second step. In the second step, the noise-tolerant hybrid input-output algorithm[38] with fixed support was applied. In both steps, we also applied the modified hybrid input-output algorithm (iterative normalization),[39] which is effective in handling missing near-forward CXD data.

Fig. 5(e) shows the sample image reconstructed from the CXD pattern in Fig. 5(a). Using results with 100 different initial random seeds, correlation coefficients were calculated between all pairs of the reconstructed images. 10 images with the highest similarity were selected and averaged to obtain the final reconstruction shown in Fig. 5(e). The reconstructed image of the self-assembly thus obtained has a diameter of about 120 nm. The full-period spatial resolution of reconstructed images estimated by using the phase retrieval transfer function[40] was 12.3 nm and each 30-nm-diameter GNP can be clearly identified. No significant difference in the structure was observed between the in-solution XFEL image in Fig. 5(e) and the dried STEM image in Fig. 5(f) indicating that the self-assembly has a relatively rigid structure. Measured dried STEM images, however, contained some self-assemblies with a certain degree of deformation. More generally, self-assemblies in solutions are fragile and undergo large structural changes through the drying process or the interaction with the substrate,[41,42] which may cause the loss of their functions. Imaging of intact structures and dynamics in solution is thus important. It is also not obvious whether self-assemblies can retain their structure when ejected using sample injectors widely used in XFEL based CDI studies.

VII. CONCLUSION AND OUTLOOK

In conclusion, we designed and fabricated MLEAs for XFEL based CDI of solution samples under controlled environmental conditions. A semi-automated MLEA assembling system was also developed for efficient sample preparation. We confirmed that each enclosure can maintain solution samples even when a neighboring enclosure is broken under a vacuum. We performed PCXSS measurement for self-assembled GNPs in solution enclosed in MLEAs and reconstructed the sample snapshot at 12.3 nm resolution. The single-particle hit rate was 31% and is not far from the theoretical upper limit of 37% derived from the Poisson statistics. The high hit rate with MLEAs can contribute to the reduction of the sample solution consumption, which is especially important when measuring samples with high scarcity value. MLEAs can be usefully applied also for PCXSS measurement of various samples[42,43] including live bacterial cells.[24] It is also interesting to perform PCXSS measurement under various environmental conditions including time-resolved measurement triggered by external stimuli.

We presented here an imaging result of submicrometer-sized objects using a micrometer-focused XFEL beam. A more tightly focused XFEL beam with higher fluence will enable single-particle imaging (SPI) of smaller objects, such as biological supramolecular complexes. Such measurement will become possible with an X-ray focusing optics with a large numerical aperture.[44,45] To achieve a higher hit rate with tightly focused XFEL beams, it is advantageous to be able to easily increase the solution concentration in MLEAs. However, in order to employ MLEAs for SPI of smaller objects, it is necessary to suppress background scattering from solvents and membrane windows. To this end, we are developing MLEAs using graphene windows. One of the ultimate goals is to create lipid bilayer chambers[46] in MLEAs and observe active embedded membrane proteins in solution.[47]

ACKNOWLEDGMENTS

The XFEL experiments were performed at SACLA with the approval of the Japan Synchrotron Radiation Research Institute (JASRI) (Proposal Nos. 2019B8016, 2019A8023, 2018B8025, 2018A8047, 2017B8061, 2017A8006, 2016B8065, 2016A8049, 2015B8050, 2015A8052, 2014B8053, 2014A8035, 2013B8051, 2013A8046, 2012B8039, and 2012A8034). The phase retrieval analysis was carried out using the Mini-K supercomputer and HPC system at the SACLA facility (Proposal Nos. 2018A8047, 2017B8061, 2017A8006, 2016B8065, 2016A8049, 2015B8050, 2015A8052, and 2014B8053). We thank the operation and engineering staff of SACLA for helping perform the PCXSS experiment, the Nanotechnology Platform Program of MEXT for helping perform MLEA fabrication, and M. Kusuzaki for fabricating jigs to seal MLEAs. This work was supported by JSPS KAKENHI 15H05737, 16H05989, 16K01942, 16K05527, 17H04819, and 20H05433; JST PRESTO JPMJPR1772; the X-ray Free Electron Laser Priority Strategy Program of MEXT; and the Research Program of "Five-star Alliance" and the Cooperative Research Program of "NJRC Mater. & Dev." Support by the "Photoexcitonix Project" in Hokkaido University is also acknowledged.

AIP PUBLISHING DATA SHARING POLICY

The data that support the findings of this study are available from the corresponding author upon reasonable request.

REFERENCES

1. C. Y. J. Hémonnot and S. Köster, ACS Nano **11**, 8542−8559 (2017).
2. J. Pine and J. R. Gilbert, in *X-ray Microscopy III (Springer Series in Optical Sciences, Vol. 67)*, edited by A. Michette, G. Morrison, and C. Buckley, pp. 388–391 (Springer-Verlag, Berlin Heidelberg, 1992).
3. K. K. Goncz, P. Batson, D. Ciarlo, B. W. Loo Jr, S. S. Rothman, J. Microsc. **168**, 101−110 (1992).
4. D. Nam, J. Park, M. Gallagher-Jones, S. Kim, S. Kim, Y. Kohmura, H. Naitow, N. Kunishima, T. Yoshida, T. Ishikawa, and C. Song, Phys. Rev. Lett. **110**, 098103 (2013).
5. M. Bartels, M. Krenkel, J. Haber, R. N. Wilke, and T. Salditt, Phys. Rev. Lett. **114**, 048103 (2015).
6. N. Strelnikova, N. Sauter, M. Guizar-Sicairos, M. Göllner, A. Diaz, P. Delivani, M. Chacón, I. M. Tolić, V. Zaburdaev, and T. Pfohl, Sci. Rep. **7**, 13775 (2017).
7. B. Weinhausen and S. Köster, Lab Chip **13**, 212−215 (2013).
8. *Liquid cell electron microscopy*, edited by F. M. Ross (Cambridge University Press, New York, 2017).
9. R. Neutze, R. Wouts, D. van der Spoel, E. Weckert and J. Hajdu, Nature **406**, 752–757 (2000).
10. H. N. Chapman, A. Barty, M. J. Bogan, S. Boutet, M. Frank, S. P. Hau-Riege, S. Marchesini, B. W. Woods, S. Bajt, W. H. Benner, R. A. London, E. Plönjes, M. Kuhlmann, R. Treusch, S. Düsterer, T. Tschentscher, J. R. Schneider, E. Spiller, T. Möller, C. Bostedt, M. Hoener, D. A. Shapiro, K. O. Hodgson, D. van der Spoel, F. Burmeister, M. Bergh, C. Caleman, G. Huldt, M. M. Seibert, F. R. N. C. Maia, R. W. Lee, A. Szöke, N. Timneanu and J. Hajdu, Nat. Phys. **2**, 839–843 (2006).
11. D. Sayre, Acta Cryst. **5**, 843 (1952).
12. J. R. Fienup, Appl. Opt. **21**, 2758–2769 (1982).
13. J. Miao, P. Charalambous, J. Kirz, and D. Sayre, Nature **400**, 342–344 (1999).
14. M. J. Bogan, W. H. Benner, S. Boutet, U. Rohner, M. Frank, A. Barty, M. M. Seibert, F. Maia, S. Marchesini, S. Bajt, B. Woods, V. Riot, S. P. Hau-Riege, M. Svenda, E. Marklund, E. Spiller, J. Hajdu and H. N. Chapman, Nano Lett. **8**, 310–316 (2008).
15. M. F. Hantke, D. Hasse, F. R. N. C. Maia, T. Ekeberg, K. John, M. Svenda, N. D. Loh, A. V. Martin, N. Timneanu, D. S. D. Larsson, G. van der Schot, G. H. Carlsson, M. Ingelman, J. Andreasson, D. Westphal, M. Liang, F. Stellato, D. P. DePonte, R. Hartmann, N. Kimmel, R. A. Kirian, M. M. Seibert, K. Mühlig, S. Schorb, K. Ferguson, C. Bostedt, S. Carron, J. D. Bozek, D. Rolles, A. Rudenko, S. Epp, H. N. Chapman, A. Barty, J. Hajdu and I. Andersson, Nat. Photon. **8**, 943–949 (2014).

16. J. Bielecki, M. F. Hantke, B. J. Daurer, H. K. N. Reddy, D. Hasse, D. S. D. Larsson, L. H. Gunn, M. Svenda, A. Munke, J. A. Sellberg, L. Flueckiger, A. Pietrini, C. Nettelblad, I. Lundholm, G. Carlsson, K. Okamoto, N. Timneanu, D. Westphal, O. Kulyk, A. Higashiura, G. van der Schot, N. D. Loh, T. E. Wysong, C. Bostedt, T. Gorkhover, B. Iwan, M. M. Seibert, T. Osipov, P. Walter, P. Hart, M. Bucher, A. Ulmer, D. Ray, G. Carini, K. R. Ferguson, I. Andersson, J. Andreasson, J. Hajdu, F. R. N. C. Maia, Sci. Adv. **5**, eaav8801 (2019).
17. A. Aquila, A. Barty, C. Bostedt, S. Boutet, G. Carini, D. dePonte, P. Drell, S. Doniach, K. H. Downing, T. Earnest, H. Elmlund, V. Elser, M. Gühr, J. Hajdu, J. Hastings, S. P. Hau-Riege, Z. Huang, E. E. Lattman, F. R. N. C. Maia, S. Marchesini, A. Ourmazd, C. Pellegrini, R. Santra, I. Schlichting, C. Schroer, J. C. H. Spence, I. A. Vartanyants, S. Wakatsuki, W. I. Weis and G. J. Williams, Struct. Dyn. **2**, 041701 (2015).
18. H. N. Chapman, Annu. Rev. Biochem. **88**, 35–58 (2019).
19. D. Nam, C. Kim, Y. Kim, T. Ebisu, M. Gallagher-Jones, J. Park, S. Kim, S. Kim, K. Tono, D. Y. Noh, M. Yabashi, T. Ishikawa, and C. Song, J. Phys. B **49**, 034008 (2016).
20. J. Fan, Z. Sun, Y. Wang, J. Park, S. Kim, M. Gallagher-Jones, Y. Kim, C. Song, S. Yao, J. Zhang, J. Zhang, X. Duan, K. Tono, M. Yabashi, T. Ishikawa, C. Fan, Y. Zhao, Z. Chai, X. Gao, T. Earnest, and H. Jiang, Sci. Rep. **6**, 34008 (2016).
21. A. Kobayashi, Y. Sekiguchi, T. Oroguchi, K. Okajima, A. Fukuda, M. Oide, M. Yamamoto and M. Nakasako, J. Synchrotron Rad. **23**, 975–989 (2016).
22. I. Martiel, H. M. Müller-Werkmeister and A. E. Cohen, Acta Cryst. D **75**, 160–177 (2019).
23. T. Ishikawa *et al.*, Nat. Photon. **6**, 540–544 (2012).
24. T. Kimura, Y. Joti, A. Shibuya, C. Song, S. Kim, K. Tono, M. Yabashi, M. Tamakoshi, T. Moriya, T. Oshima, T. Ishikawa, Y. Bessho and Y. Nishino, Nat. Commun. **5**, 3052 (2014).
25. J. Pérez and Y. Nishino, Curr. Opin. Struct. Biol. **22**, 670–678 (2012).
26. T. Nakane, Y. Joti, K. Tono, M. Yabashi, E. Nango, S. Iwata, R. Ishitani, and O. Nureki, J. Appl. Cryst. **49**, 1035–1041 (2016).
27. M. J. Berger, J. H. Hubbell, S. M. Seltzer, J. Chang, J. S. Coursey, R. Sukumar, D. S. Zucker, and K. Olsen, XCOM: Photon Cross Section Database (version 1.5) (2010).
http://physics.nist.gov/xcom
National Institute of Standards and Technology, Gaithersburg, MD, USA.
28. *Theory of plates and shells*, 2nd ed., S. Timoshenko and S. Woinowsky-Krieger (McGraw-Hill, New York, 1964).
29. DIN EN 843-2:2007 (2007).
30. H. Yumoto, H. Mimura, T. Koyama, S. Matsuyama, K. Tono, T. Togashi, Y. Inubushi, T. Sato, T. Tanaka, T. Kimura, H. Yokoyama, J. Kim, Y. Sano, Y. Hachisu, M. Yabashi, H. Ohashi, H. Ohmori, T. Ishikawa and K. Yamauchi, Nat. Photonics **7**, 43–47 (2013).
31. C. Song, K. Tono, J. Park, T. Ebisu, S. Kim, H. Shimada, S. Kim, M. Gallagher-Jones, D. Nam, T. Sato, T. Togashi, K. Ogawa, Y. Joti, T. Kameshima, S. Ono, T. Hatsui, S. Iwata, M. Yabashi and T.

Ishikawa, J. Appl. Crystallogr. **47**, 188–197 (2014).

32. T. Kameshima, S. Ono, T. Kudo, K. Ozaki, Y. Kirihara, K. Kobayashi, Y. Inubushi, M. Yabashi, T. Horigome, A. Holland, K. Holland, D. Burt, H. Murao and T. Hatsui, Rev. Sci. Instrum. **85**, 033110 (2014).
33. Y. Joti, T. Kameshima, M. Yamaga, T. Sugimoto, K. Okada, T. Abe, Y. Furukawa, T. Ohata, R. Tanaka, T. Hatsui and M. Yabashi, J. Synchrotron Radiat. **22**, 571–576 (2015).
34. J. Wei, H. Mitomo, T. Tani, Y. Matsuo, K. Niikura, M. Naya, and K. Ijiro, Langmuir **34**, 12445–12451 (2018).
35. K. Niikura, N. Iyo, Y. Matsuo, H. Mitomo, and K. Ijiro, ACS Appl. Mater. Interfaces **5**, 3900–3907 (2013).
36. D. Russell Luke, Inverse Problem **21**, 37–50 (2005).
37. S. Marchesini, H. He, H. N. Chapman, S. P. Hau-Riege, A. Noy, M. R. Howells, U. Weierstall, and J. C. H. Spence, Phys. Rev. B **68**, 140101(R) (2003).
38. A. V. Martin, F. Wang, N. D. Loh, T. Ekeberg, F. R. N. C. Maia, M. Hantke, G. van der Schot, C. Y. Hampton, R. G. Sierra, A. Aquila, S. Bajt, M. Barthelmess, C. Bostedt, J. D. Bozek, N. Coppola, S. W. Epp, B. Erk, H. Fleckenstein, L. Foucar, M. Frank, H. Graafsma, L. Gumprecht, A. Hartmann, R. Hartmann, G. Hauser, H. Hirsemann, P. Holl, S. Kassemeyer, N. Kimmel, M. Liang, L. Lomb, S. Marchesini, K. Nass, E. Pedersoli, C. Reich, D. Rolles, B. Rudek, A. Rudenko, J. Schulz, R. L. Shoeman, H. Soltau, D. Starodub, J. Steinbrener, F. Stellato, L. Strüder, J. Ullrich, G. Weidenspointner, T. A. White, C. B. Wunderer, A. Barty, I. Schlichting, M. J. Bogan, and H. N. Chapman, Opt. Express. **20**, 16650–16661 (2012).
39. Y. Nishino, J. Miao, and T. Ishikawa, Phys. Rev. B **68**, 220101(R) (2003).
40. H. N. Chapman, A. Barty, S. Marchesini, A. Noy, S. P. Hau-Riege, C. Cui, M. R. Howells, R. Rosen, H. He, J. C. H. Spence, U. Weierstall, T. Beetz, C. Jacobsen and D. Shapiro, J. Opt. Soc. Am. A **23**, 1179–1200 (2006).
41. S. Nakamura, H. Mitomo, M. Aizawa, T. Tani, Y. Matsuo, K. Niikura, A. Pike, M. Naya, A. Shishido, and K. Ijiro, ACS Omega **2**, 2208–2213 (2017).
42. J. Wei, K. Niikura, T. Higuchi, T. Kimura, H. Mitomo, H. Jinnai, Y. Joti, Y. Bessho, Y. Nishino, Y. Matsuo and K. Ijiro, J. Am. Chem. Soc. **138**, 3274–3277 (2016).
43. R. Iida, H. Kawamura, K. Niikura, T. Kimura, S. Sekiguchi, Y. Joti, Y. Bessho, H. Mitomo, Y. Nishino and K. Ijiro, Langmuir **31**, 4054–4062 (2015).
44. T. Koyama, H. Yumoto, T. Kimura, A. Suzuki, T. Kameshima, Y. Joti, K. Tono, N. Tani, T. Tachibana, Y. Konishi, Y. Bessho, Y. Nishino, M. Yabashi, and H. Ohashi, Microsc. Microanal. **24**(Suppl 2), 294–295 (2018).
45. H. Yumoto *et al.*, in preparation (2020).
46. R. Watanabe, N. Soga, D. Fujita, K. V. Tabata, L. Yamauchi, S. H. Kim, D. Asanuma, M. Kamiya, Y. Urano, H. Suga and H. Noji, Nat. Commun. **5**, 4519 (2014).
47. A. Suzuki, T. Kimura, Y. Yang, Y. Niida, A. Nishioka, T. Tachibana, M. Takei, K. Tono, M.

Yabashi, T. Ishikawa, T. Oshima, Y. Bessho, Y. Joti, and Y. Nishino, Phys. Chem. Chem. Phys. **22**, 2622–2628 (2020).

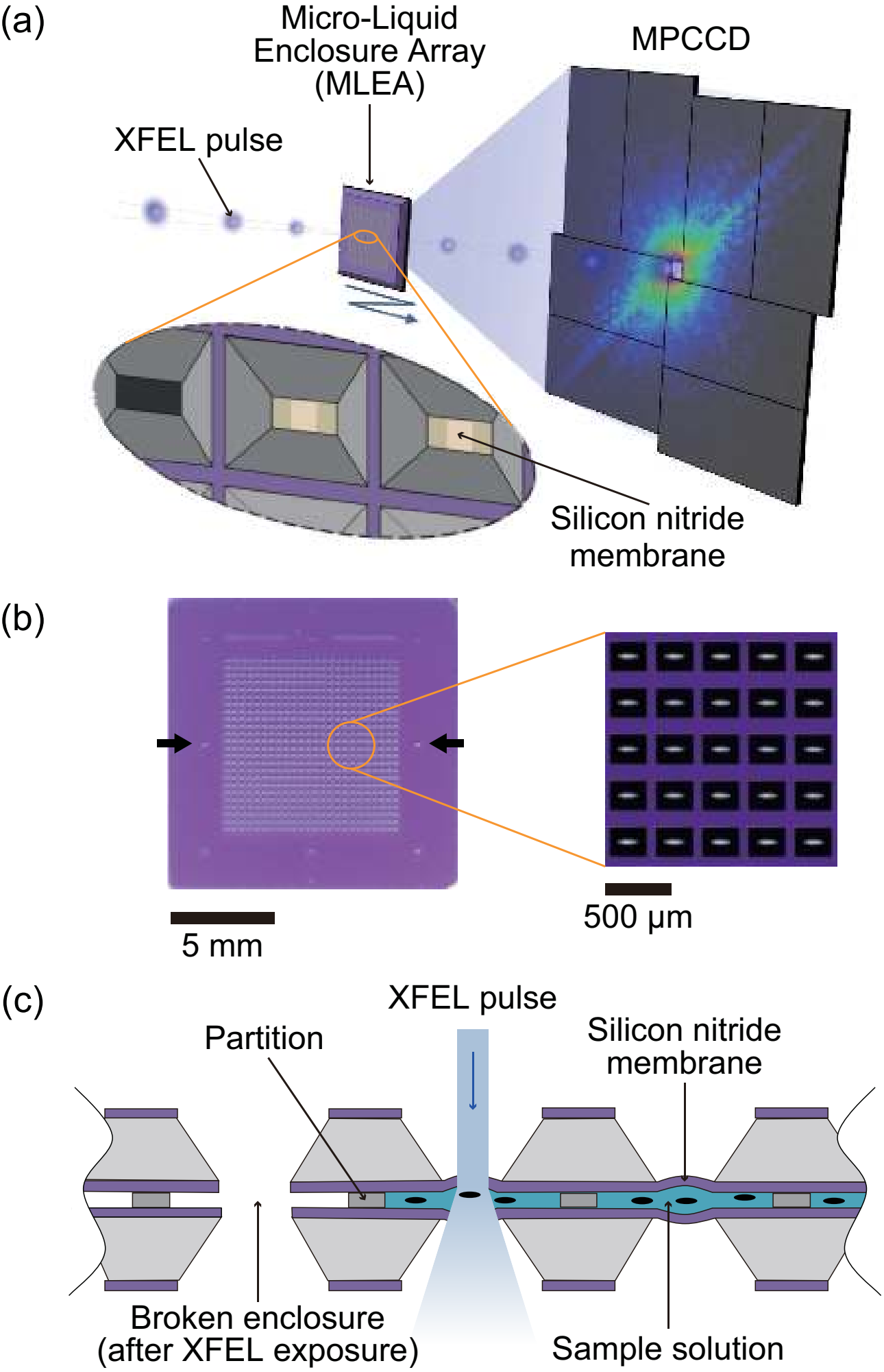
(a)
Micro-Liquid Enclosure Array (MLEA)
MPCCD
XFEL pulse
Silicon nitride membrane
(b)
5 mm
500 μm
(c)
XFEL pulse
Partition
Silicon nitride membrane
Broken enclosure (after XFEL exposure)
Sample solution

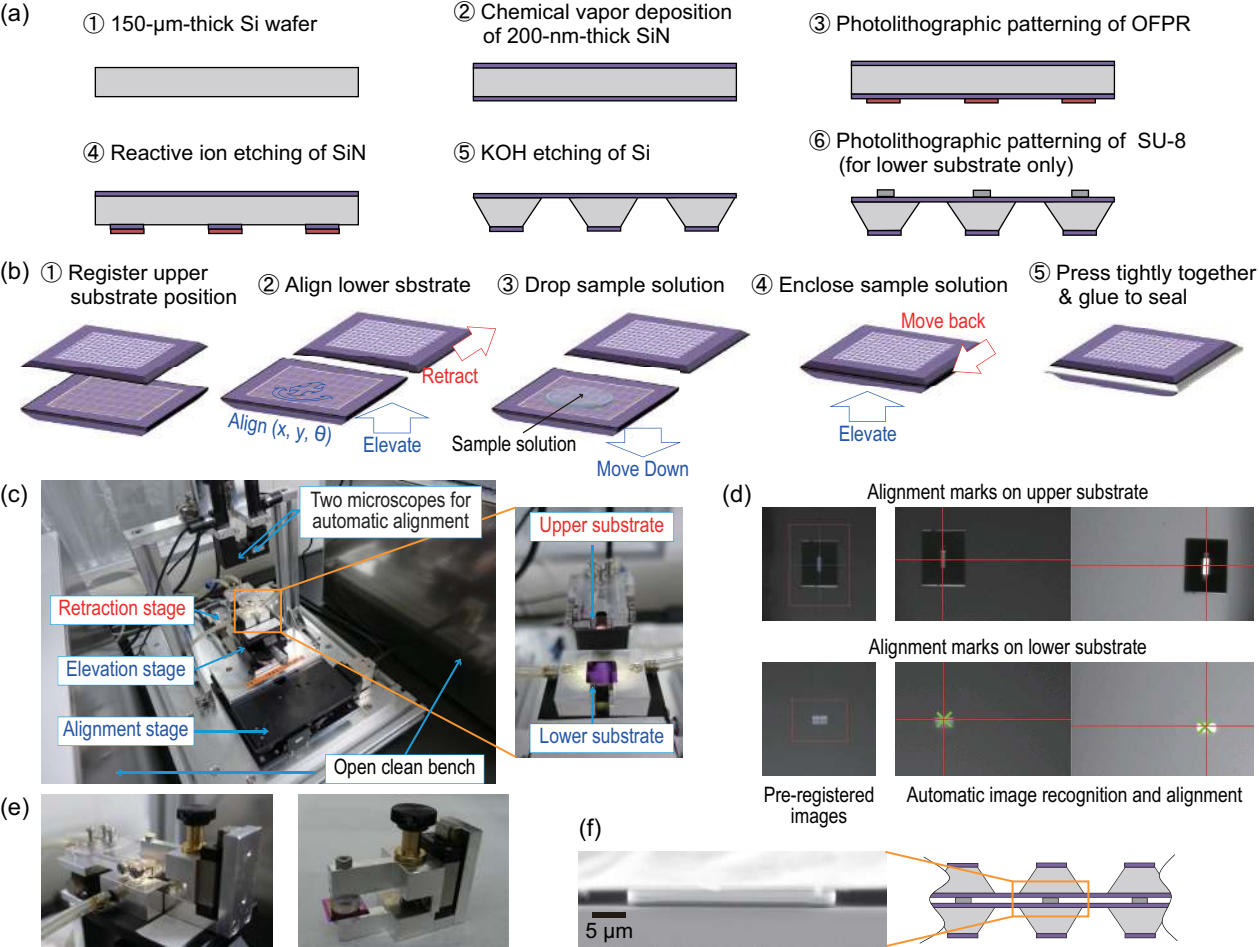
(a)
① 150-μm-thick Si wafer
② Chemical vapor deposition of 200-nm-thick SiN
③ Photolithographic patterning of OFPR
④ Reactive ion etching of SiN
⑤ KOH etching of Si
⑥ Photolithographic patterning of SU-8 (for lower substrate only)
(b)
① Register upper substrate position
② Align lower sbstrate
③ Drop sample solution
④ Enclose sample solution
⑤ Press tightly together & glue to seal
Retract
Align (x, y, θ)
Elevate
Sample solution
Move Down
Move back
Elevate
(c)
Two microscopes for automatic alignment
Upper substrate
Retraction stage
Elevation stage
Alignment stage
Lower substrate
Open clean bench
(d)
Alignment marks on upper substrate
Alignment marks on lower substrate
Pre-registered images
Automatic image recognition and alignment
(e)
(f)
5 μm

(a)

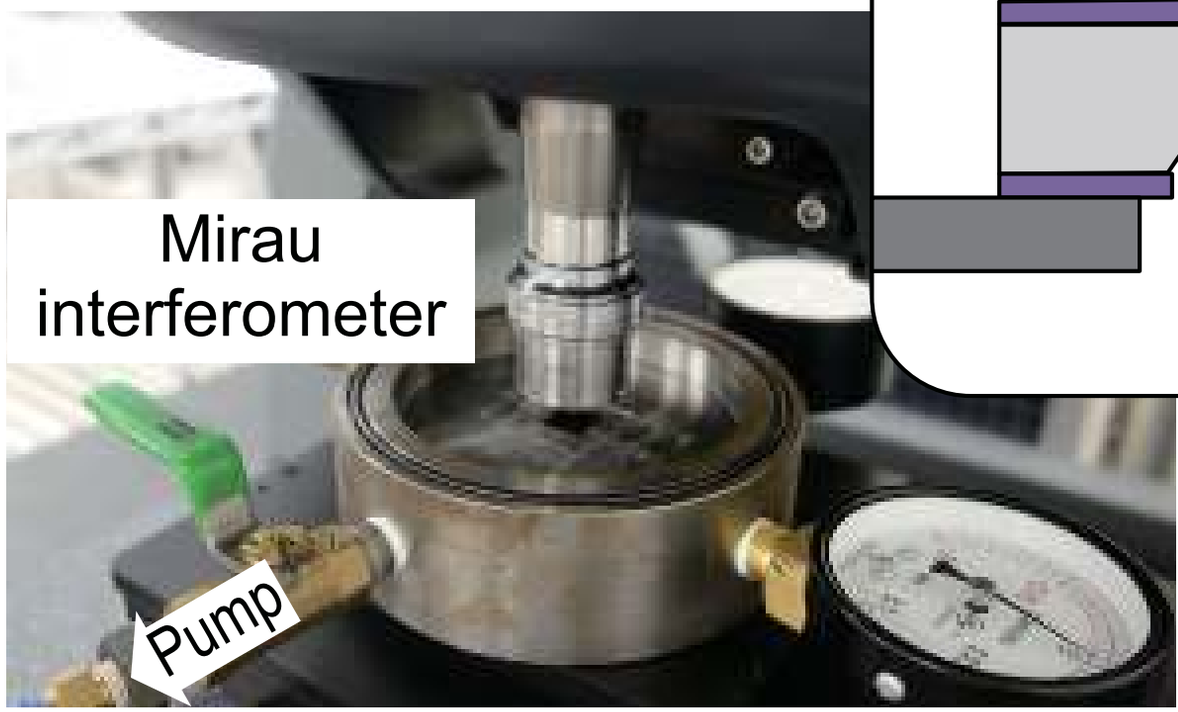
Mirau
interferometer
Pump

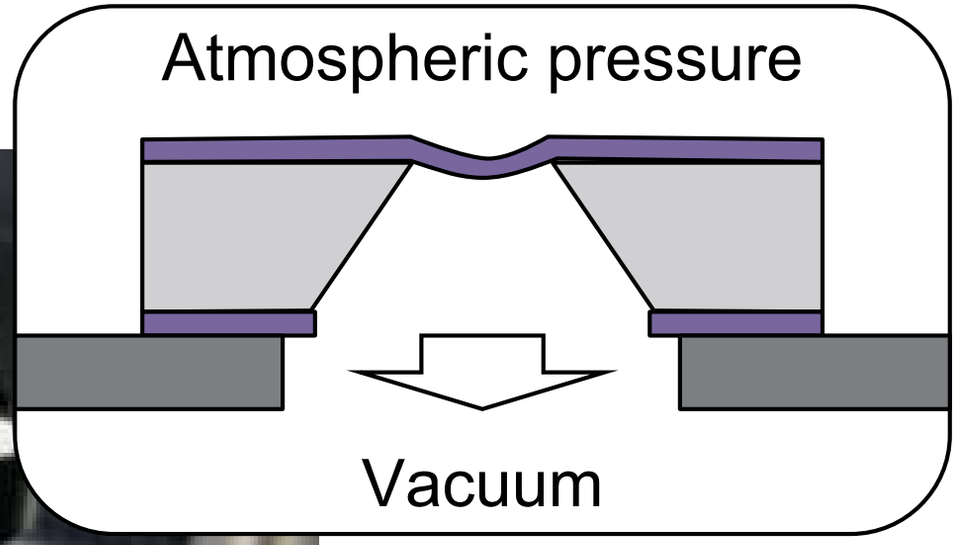
Atmospheric pressure
Vacuum

(b)

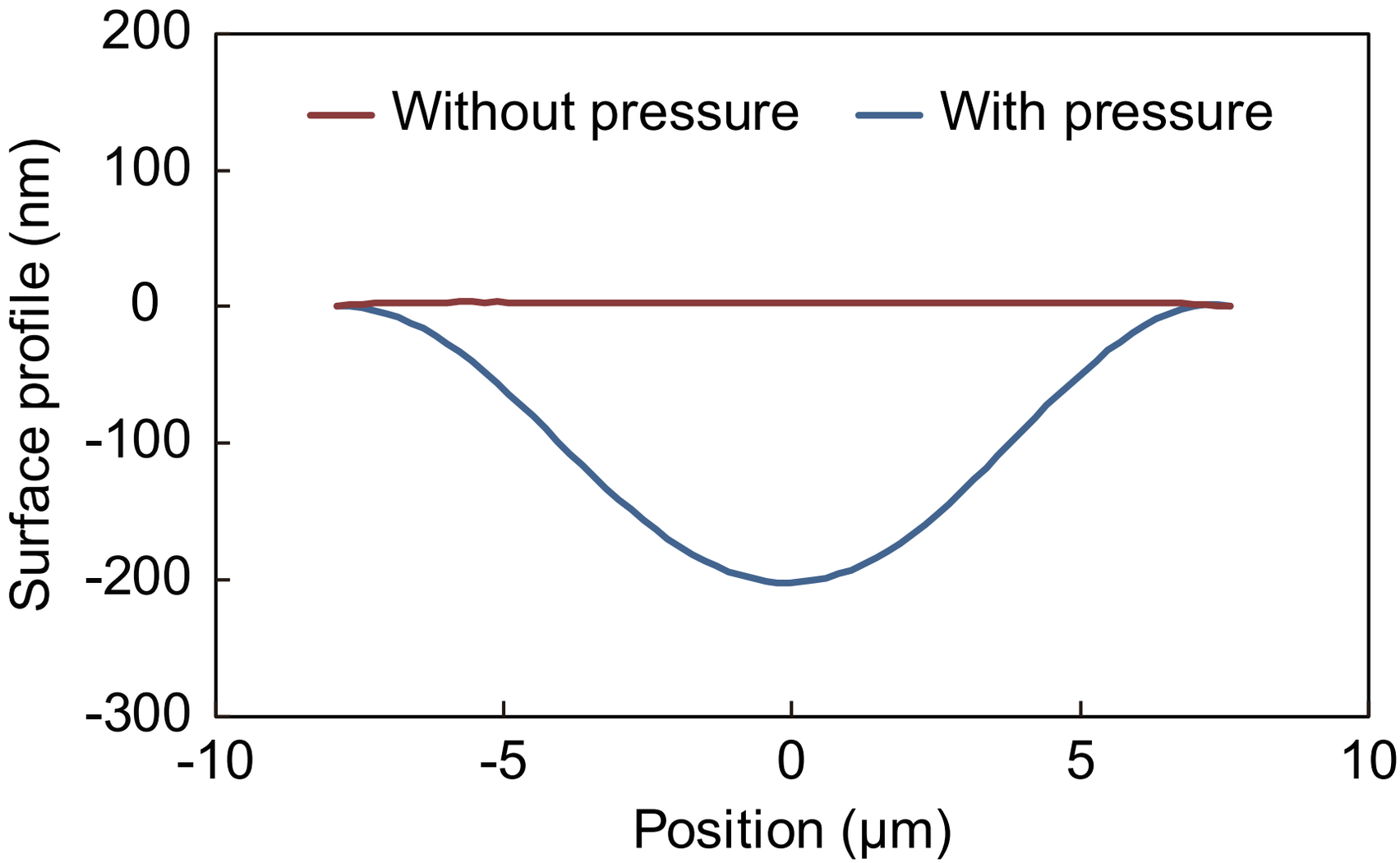
Without pressure
With pressure
Surface profile (nm)
200
100
0
-100
-200
-300
-10
-5
0
5
10
Position (μm)

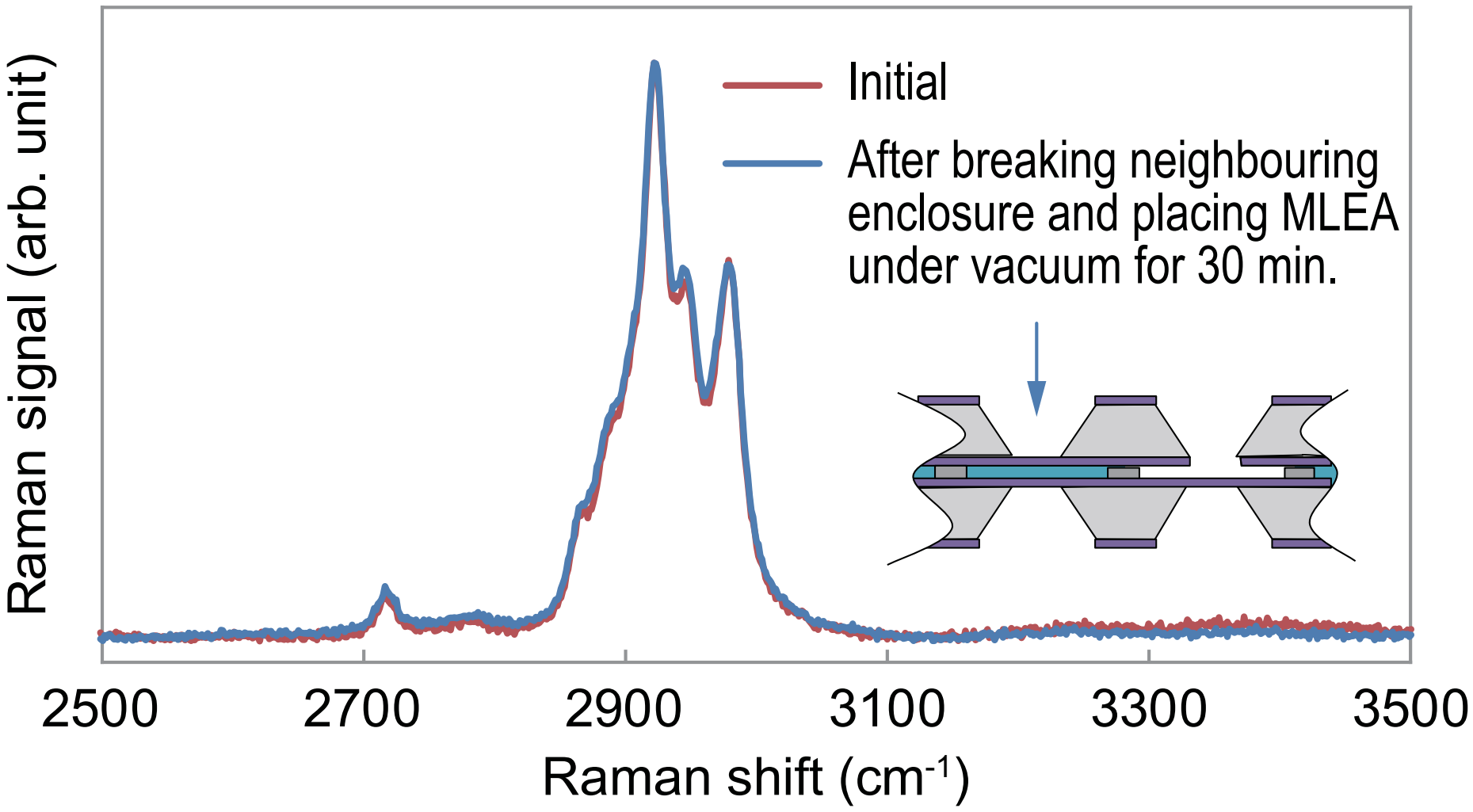
Initial
After breaking neighbouring enclosure and placing MLEA under vacuum for 30 min.
Raman signal (arb. unit)
2500
2700
2900
3100
3300
3500
Raman shift (cm-1)

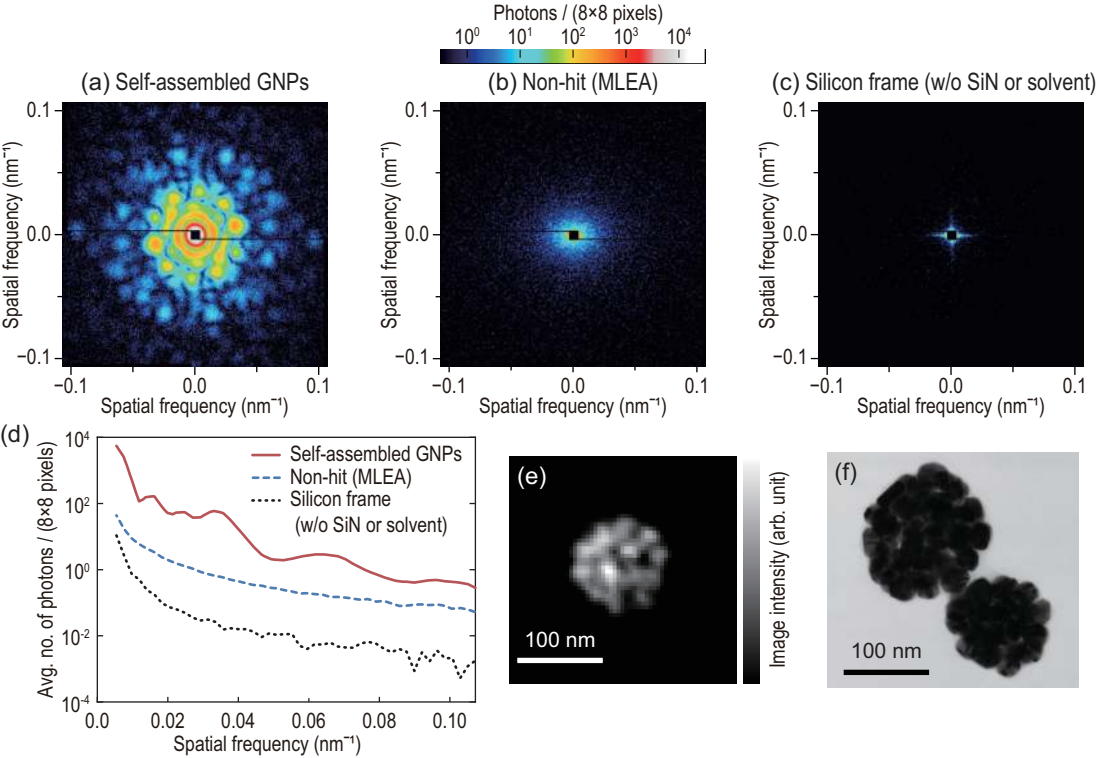
Photons / (8×8 pixels)
10^0 10^1 10^2 10^3 10^4
(a) Self-assembled GNPs
(b) Non-hit (MLEA)
(c) Silicon frame (w/o SiN or solvent)
Spatial frequency (nm^{-1})
0.1
0.0
−0.1
(d)
Avg. no. of photons / (8×8 pixels)
10^4
10^2
10^0
10^{-2}
10^{-4}
Self-assembled GNPs
Non-hit (MLEA)
Silicon frame
(w/o SiN or solvent)
0.0 0.02 0.04 0.06 0.08 0.10
Spatial frequency (nm^{-1})
(e)
100 nm
Image intensity (arb. unit)
(f)
100 nm